Arrhenius Photobases and Their Application to CO_2 Capture

Michael Purdy,[a] Ariel Y. Wang,[a] Matthew C. Drummer,[a] Daniel G. Nocera,[a] Richard Y. Liu*[,a]

[a]Department of Chemistry and Chemical Biology, Harvard University, 12 Oxford St., Cambridge, MA 02138, United States

*Correspondence by e-mail to: richardliu@chemistry.harvard.edu

Abstract

Leading strategies for the capture of CO_2 from point sources and directly from the atmosphere confront the challenge of high energy costs for thermal sorbent regeneration. In response, photochemical processes driven by sunlight as the sole external stimulus have recently been advanced as a promising alternative. Although many examples of light-induced pH swings using metastable photoacids have been reported, the complementary mode of operation, using photoswitchable bases, has not been extensively considered due in part to the rarity of photobases that can support large, reversible pH jumps in water. Here, we report the design of fluorenol-based Arrhenius photobases that take advantage of excited-state aromaticity and ground-state antiaromaticity to generate large basicity swings (nearly 6 pH units) with high reversibility (*ca.* 1% degradation per cycle). The system is stable to oxygen, can be driven by natural sunlight, and is shown to concentrate CO_2 from ambient air. To understand the high efficiency (>20% photochemical quantum yield) of hydroxide release, the mechanism of C–O dissociation was elucidated using transient-absorption spectroscopy. This study provides a general framework for the design of photoreversible aqueous bases and guiding principles for their usage in solar-powered CO_2 management.

Introduction

As the most significant driver of anthropogenic climate change, atmospheric CO_2 needs to be dramatically reduced to avoid catastrophic future scenarios.[1–3] Hence, chemical systems for removing CO_2 from emission streams and even directly from the atmosphere (direct air capture, DAC) are of practical significance.[4–7] Leading technologies rely on nucleophilic solvents such as alkaline aqueous solutions and amines (*e.g.*, ethanolamine) or on porous sorbents with nucleophilic functionalities, both

of which form strong covalent adducts with CO_2.[8,9] To regenerate the stationary phase and release the captured CO_2, energy-intensive thermal stripping is the most popular method.[10] Though these systems are becoming increasingly efficient and scalable, there is considerable interest in alternative approaches using materials that cycle between capture and release modes using nonthermal stimuli, including applied electrical potentials,[11] humidity swings,[12] microwave irradiation,[13] and photochemistry.[14] These newer approaches can in principle have advantages in terms of energy efficiency, but the underlying thermodynamic and molecular-design principles are substantially less developed than for thermally driven systems.

Switchable organic molecules regulated by visible light have attracted attention recently in this context, specifically those that reversibly release protons, such as spiropyran photochromes, which we and others have examined for reversible CO_2 capture.[14–17] By directly converting solar energy and thus avoiding the intermediate generation, storage, and distribution of clean electricity, photochemical separations could eventually be efficient and distributable options for some applications, although dramatic increases in photon utilization, stability, and capture/release kinetics are still required. Furthermore, while photoacids demonstrate important fundamental principles for coupling photoswitching with light-independent equilibria, their inability to operate at high pH is a fundamental limitation inasmuch as they can only capture CO_2 from concentrated streams and are likely inapplicable for DAC without additional alkaline sorbents.[17]

As part of our research on direct light-driven separations, we considered whether the opposite mode of operation, involving *photobases* that display reversible photon-induced release of hydroxide, might represent a more promising mechanism for carbon capture. An especially appealing aspect of such a scheme is that the photochemical step (hydroxide release) is unimolecular and CO_2-independent and therefore, may proceed with high quantum efficiencies with the judicious design of the photobase. In contrast, we have shown that photoacidic mechanisms necessarily involve, after light-triggered proton release, a competition between bimolecular proton recapture by the dye and bicarbonate protonation.[14] A further advantage of a photobasic scheme is that high concentrations of hydroxide could

be achieved with a sufficiently soluble and photoreactive dye, setting the stage for capture from dilute streams.

Electrochemically switched systems have been reported that depend on the reversible generation of hydroxide and corresponding pH swing in the alkaline direction.[11,18–20] Solutions containing redox-active bases, such as phenazines, have been shown to undergo large pH increases upon reduction, enabling separation of CO_2 from very dilute streams.[21–23] A major limitation of electrochemical strategies is the oxygen-instability of many reduced species in aqueous solution, although promising progress has been made using alcohol additives in organic solvent.[23,24] We postulated that a photoswitchable base could in principle achieve similar cyclic pH swings in aqueous solution without the problems of oxygen sensitivity nor the requirement for electrochemical apparatus such as cells, membranes, electrodes, and supporting electrolytes. However, while metastable-state photoacids such as merocyanines have been continuously optimized over the past decades, and extensive physical-organic studies have been performed on their use as photoswitchable buffers,[25] analogous research on switchable photobases is rather limited. Several Brønsted photobases, mainly consisting of quinolines and acridines, have been discovered, and Lukas *et al.* showed a guanidine Brønsted photobase could form reversible adducts with CO_2 in acetonitrile solution using light. However, Brønsted photobases predominantly function in organic solvent, rely on UV light and exhibit small shifts in pK_a (~2 units), thereby limiting their utility in reversible CO_2 capture.[26–30]

In this work, we show that a new class of reversible hydroxide emitters, 9-aryl-9-fluorenols, represent among the first highly reversible and tuneable Arrhenius photobases, capable of generating large pH swings reaching *ca*. pH 12 under illumination. We report the effect of ground state pK_a on the efficiency of capture and release, validating a precise pH-matching principle that we had developed in the context of photoacids.[14] Solutions of these materials can capture CO_2 from streams as dilute as 400 ppm and then release that captured CO_2 upon removal of the light source, resulting in output concentrations that are significantly higher than the input stream. Studies into the effects of excited-state aromaticity, ground-state antiaromaticity, and the transient dynamics provide insight into the

design principles underlying the effectiveness of these photobases for reversible CO_2 capture compared to previously known hydroxide emitters.

Results and Discussion

Malachite green derivatives and attempted acidity tuning

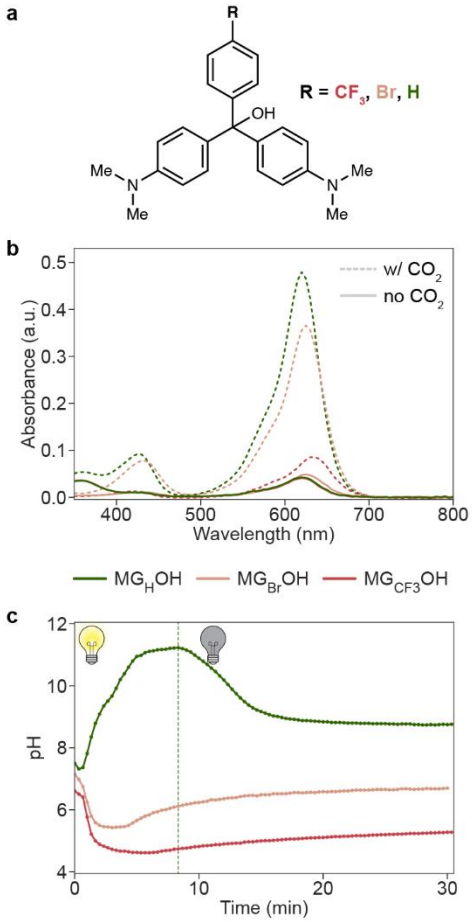

Figure 1. *Investigation of **MGCB** derivatives for reversible CO_2 capture.* (a) *Para*-substituted **MGCB** derivatives evaluated. (b) Carbocation growth from $\mathbf{MG_ROH}$ photobases, 1 mM in 2:1 MeCN:H_2O solution (solvent ratio used hereafter unless otherwise stated) after exposure to 1 atm CO_2 for 2 min in darkness and equilibration for 30 min. An aliquot was diluted to 10 μM and the UV-vis absorption spectrum recorded to detect carbocation ($\mathbf{MG_R^+}$) growth (dashed lines, λ_{det} ~ 620 nm). (c) Change in the pH of 1 mM solution of $\mathbf{MG_ROH}$ photobases upon photoirradiation (λ_{exc} = 254 nm) . Once the pH remained stagnant for 3 min, the light source was removed (dashed line), and the pH change recorded.

Acridinols, trityl alcohols, and fluorenols are examples of molecular switches that photochemically and reversibly release hydroxide.[31–34] The best-known Arrhenius photobase, malachite green carbinol base (**MGCB**), reported by Irie in 1982, was found to engender large reversible pH swings by toggling between a neutral alcohol state and photoionized ion pair of a trityl carbocation and

hydroxide, formed upon C–O heterolysis.[34] This behaviour has been used to effect conformational changes in DNA/RNA and in light-driven drug-release applications, but otherwise, limited follow-up work has been published.[35–37] We wondered whether the photoinduced pH swing of **MGCB** could be utilised to reversibly capture CO_2 and accordingly, our attempts initially focused on engineering the structure of **MGCB** to satisfy the criteria of efficient CO_2 capture under photoirradiation and CO_2 release in darkness (**Figure 1a**).

A 1 mM solution of $\mathbf{MG_HOH}$ in 2:1 MeCN/water was irradiated with UV light (λ_{exc} = 254 nm) under rapid stirring, resulting in a pH jump from 7.0 to 10.8 over the course of 5 min (**Figure 1c**, green trace). Upon removal of the light source, the solution pH decreased to 8.7 over the next 5 min. Thus, $\mathbf{MG_HOH}$ undergoes significant but not complete photodissociation in response to UV light and partial recombination in the dark suggesting its promise for the development of photoreversible CO_2 capture. However, when $\mathbf{MG_HOH}$ solutions were exposed to CO_2 (1 atm) *in the dark*, a large and irreversible prompt absorbance at 620 nm was observed that is characteristic of the corresponding carbocation (**Figure 1b**, green trace).[38] The carbocation evolution indicates the transfer of hydroxide from $\mathbf{MG_HOH}$ to CO_2, generating a carbocation-bicarbonate ion pair. Thus, $\mathbf{MG_HOH}$ is too basic and is thermodynamically unlikely to release CO_2 in the absence of illumination. In line with this supposition, a spectrophotometric titration (SI **Figure 3**) determined the pK_{aH}' of $\mathbf{MG_HOH}$ to be 6.8. We sought to reduce the pK_{aH}' by destabilising the carbocation *via para*-functionalization of the phenyl group with electron-withdrawing substituents, Br and CF_3. Whereas $\mathbf{MG_{Br}OH}$ solutions (1 mM in 2:1 MeCN/water) exposed to CO_2 (1 atm) in the dark also exhibited carbocation formation (**Figure 1b**, orange trace), $\mathbf{MG_{CF3}OH}$, was less reactive with CO_2 in the absence of light (**Figure 1b**, red trace). Aiming to evaluate whether photodissociation would proceed with these derivatives, we subjected $\mathbf{MG_{Br}OH}$ and $\mathbf{MG_{CF3}OH}$ (1 mM in 2:1 MeCN/water) to UV light (λ_{exc} = 265 nm). Unexpectedly, instead of the photobasic behaviour characteristic of parent **MGCB** ($\mathbf{MG_HOH}$), both solutions displayed a rapid decrease in pH, which appeared to slightly reverse upon removal of the light source (**Figure 1c**, red and orange traces). The photoacidity appears to be oxygen-dependent, suggesting the presence of a radical pathway that may generate hydrogen peroxide and/or organic hydroperoxides,

though these products remain to be fully characterized. Nonetheless, such complications indicated that straightforward electronic tuning of **MGCB** derivatives was unlikely to realize reversible CO_2 capture and release.

New fluorene-containing carbinol photobases

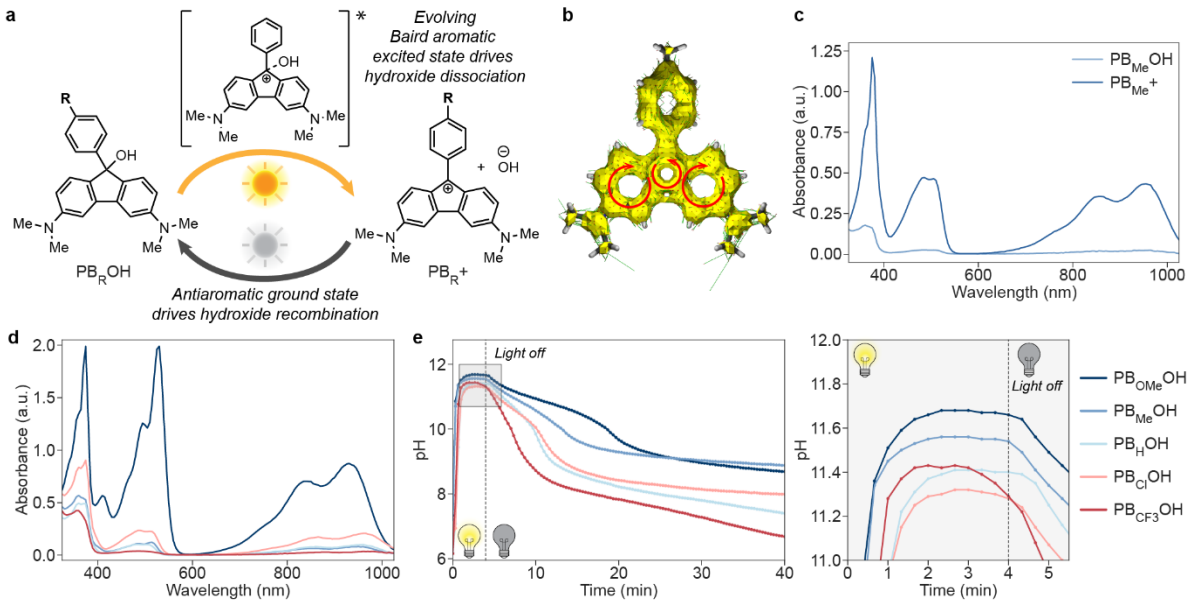

Figure 2. *Design and characterization of fluorenol photobases.* (a) Enhanced conjugation of fluorene photobases allows for excitation under visible light (λ_{exc} = 390 nm). Formation of a Baird-aromatic excited state drives charge separation, whereas the antiaromatic ground state of the cation promotes hydroxide recombination. (b) ACID plot of ground state antiaromatic carbocation. Direction of flow of current density vectors are indicated with red arrows. (c) UV-vis profile of **$PB_{Me}OH$** photobase and corresponding carbocation **PB_{Me}^+**. (d) UV-vis profile of substituted fluorene photobases after CO_2 exposure. (e) Change in pH upon photoirradiation. Photobases were stirred under visible light (λ_{exc} = 390 nm) and the pH tracked over time. The light source then was removed (indicated by dotted line) and pH decay recorded. The inset graphic (grey box) highlights the change in pH between 11 and 12.

As an alternative strategy to destabilize the trityl cation formed upon hydroxide dissociation (**Figure 2a**), we were interested in the introduction of antiaromaticity by connecting two of the aromatic rings into a fluorene substructure. Upon hydroxide dissociation, the fluorenyl cation core contains a 4π-electron cyclopentadienyl substructure, which could favour ion recombination and hence lower the pK_{aH}'. This approach has several appealing secondary consequences. First, the enhanced conjugation of the fluorene core, which effectively enforces two of the benzene rings to be coplanar, bathochromically shifts the photobase absorption to enable the system to be driven by visible light,

rather than the ultraviolet wavelengths used to operate Malachite green derivatives. Furthermore, DFT calculations in **Figure 2b** and the Supplementary Information show that, while the carbocation is indeed disfavored in the ground state, on the excited-state surface, the evolution of Baird aromaticity provides a strong thermodynamic driving force for hydroxide elimination.[38] Hence, the fluorenes may be expected to show better reversibility than their Malachite green analogues.

The parent fluorenyl photobase (**PB_HOH**) was synthesized *via* Grignard reaction of 3,6-bis(dimethylamino)fluorenone (**Figure S1**). We measured the pK_{aH}' to be 5.9 (**SI Table 1**), confirming that the effective basicity is reduced relative to **MCGB** (pK_{aH}' = 6.8). Additional tuning of the basicity was achieved by preparing derivatives substituted on the 9-aryl ring: **$PB_{CF3}OH$**, **$PB_{Cl}OH$**, **$PB_{Me}OH$**, and **$PB_{OMe}OH$**. By titration, their pK_{aH}' values spanned 2.7 units (**SI Table 1**), with the -CF_3 and -Cl *para*-substituents destabilizing the carbocation and the -Me and -OMe *para*-substituents slightly stabilizing the carbocation, but all being less basic than **MG_HOH**.

An ideal photobase must be a sufficiently weak ground-state base to avoid CO_2 capture in the dark but photodissociate a large concentration of hydroxide for maximum CO_2 capture. As shown in **Figure 2d**, only **$PB_{OMe}OH$** (pK_{aH}' = 6.7) showed significant light-independent carbocation formation after CO_2 exposure for 2 min, indicating that this candidate was too basic for reversible CO_2 capture, as would be expected from the similarity of its basicity to **MG_HOH**. Next, we evaluated the light-activated hydroxide release from each of the photobases by tracking pH of an MeCN/water solution under photoirradiation. **Figure 2e** shows the solution pH of *ca*. 7 prior to irradiation jumping to pH 11.7 and 11.6 over the course of 4 min after exposure of **$PB_{OMe}OH$** and **$PB_{Me}OH$** solutions, respectively, to a 390 nm lamp. Upon removal of the light, the pH decayed to *ca.* 8.5 over roughly 25 min, indicating quenching of over 99% of the photoeliminated hydroxide. Solutions of **PB_HOH**, **$PB_{Cl}OH$** and **$PB_{CF3}OH$** exhibited pH jumps to 11.4, 11.3, and 11.3, respectively, over 4 min of similar illumination. Subsequent resting in the dark led to pH decays to 8.0 or lower over 25 min. It is notable that **$PB_{Cl}OH$** and **$PB_{CF3}OH$** were unable to retain a steady pH under photoirradiation and some loss of hydroxide occurred before the light source was removed. We concluded that electron-withdrawing groups clearly inhibited

hydroxide ion photodissociation, and, although the effect is not as pronounced as for the **MGCB** derivatives, **$PB_{Cl}OH$** and **$PB_{CF3}OH$** were unsuitable candidates for reversible CO_2 capture.

Photoswitchable CO_2 capture and release by $PB_{Me}OH$

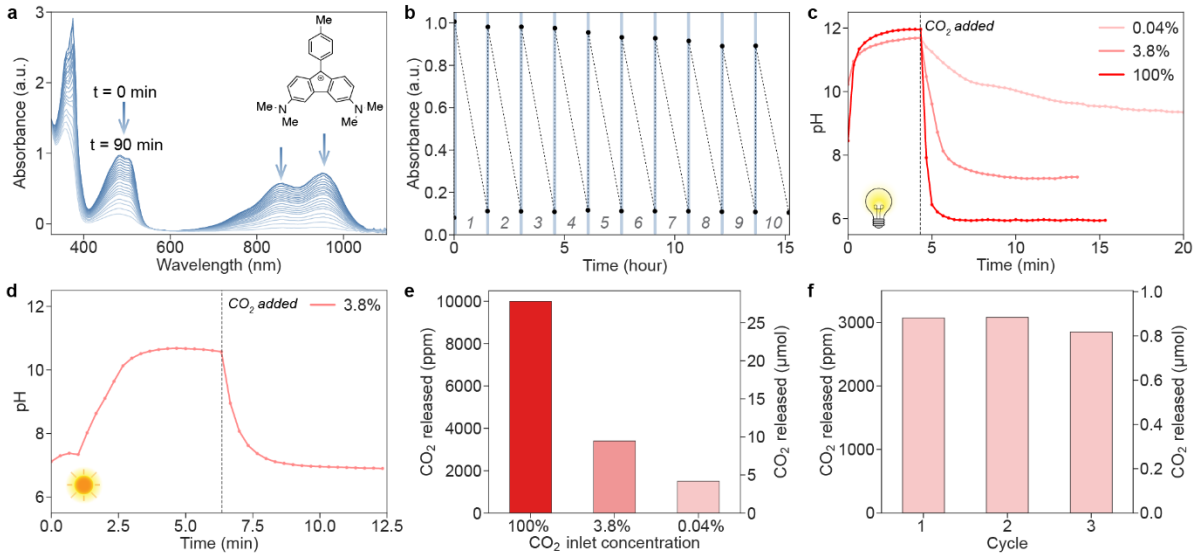

Figure 3. *Light-driven reversible CO_2 capture.* (a) Decay of photogenerated **PB_{Me}^+** cation. **$PB_{Me}OH$** solution was irradiated with 390 nm light for 1 min under stirring. UV-vis absorption of **PB_{Me}^+** was recorded periodically over 90 min, showing complete decay back to **$PB_{Me}OH$**. (b) Reversible carbocation generation was cycled 10 times over a 15-h period following the rise and decay of the 950 nm absorption peak. Solution is irradiation with 390 nm light (blue region) followed by 90 min in the dark. (c) pH changes upon CO_2 addition (dotted line) to **$PB_{Me}OH$** solutions under 390 nm light. Three different CO_2 sources were used: pure CO_2 (100%), human breath CO_2 (3.8%), and air (0.04%). (d) CO_2 addition (dotted line) to **$PB_{Me}OH$** solution under sunlight. (e) CO_2 levels detected in headspace (67 mL) after release in the dark for 90 min. (f) Cycling of direct air capture. Air was bubbled through solution for 6 min under photoirradiation and the headspace CO_2 levels (7 mL) analyzed after 90 min relaxation.

Overall, the most promising compound for reversible CO_2 capture was **$PB_{Me}OH$**, as it showed no CO_2 capture in the dark and the largest pH increase under photoirradiation. The identification of this candidate is consistent with the optimal pK_{aH}' for photobasic CO_2 capture to be *ca*. 6. An additional criterion for photobasic CO_2 capture is that the photoswitch must be stable to many cycles between the neutral and the basic ionized state. As reference, **Figure 2c** shows the absorption spectra of **$PB_{Me}OH$** and its conjugate acid **PB_{Me}^+**. Irradiating **$PB_{Me}OH$** solution with 390 nm light resulted in a large increase in carbocation absorption which gradually decayed over 90 min (**Figure 3a**). We repeated this entire experiment 10 times over a 15 h period (**Figure 3b**) and found that the maximum absorbance decreased

by only *ca*. 1% per cycle and the minimum absorbance remained unchanged, signifying an acceptable level of photostability.

We investigated the capacity of our system to capture CO_2 by tracking the pH under photoirradiation and subsequent CO_2 exposure. As shown in **Figure 3c**, solutions of **$PB_{Me}OH$** (10 mM in 2:1 MeCN/H_2O) were irradiated with a 390 nm lamp, leading to a pH jump from 7 to 11.6 over 5 min. Exposure to CO_2 streams resulted in a pH decrease as the hydroxide ions were converted to bicarbonate or carbonate, with the rate of capture and the terminal pH depending on the concentration of the input stream. First, under bubbling 100% CO_2, a near-instantaneous decline of the pH to 6.0 was observed within 1 min, indicating nearly complete utilization of the theoretical capacity. If instead, CO_2 from human exhalation (3.8% v/v) was used as the input stream, the pH decreased to 7.7 over 2 min illustrating CO_2 capture was still rapid and nearly complete (hydroxide concentration decreased by 4 orders of magnitude). Interestingly, simulated direct-air capture was successful, reaching a pH of 9.7 over a 20 min period, and continuing to decrease thereafter but very slowly. We monitored the fluorenyl carbocation concentration during this process by UV-vis spectroscopy (**SI Figure 16**), finding a gradual increase starting from the time at which air bubbling began. To our knowledge, this is the first demonstration of effective direct air capture using photogenerated hydroxide. We can estimate by charge balance that *ca*. 99% of hydroxide for capture was effectively utilized. Although a calibrated lamp was used for the test experiments above, the system can also be driven by natural sunlight. After exposing the photobase solution to direct sunlight (**Figure 3d)**, a pH increase was observed after only 3 min, although to a slightly lower terminal value (10.8). Exposure to a 3.8% CO_2/air stream again led to pH decrease to 7.0 indicating effectively complete neutralization of all hydroxide ions by reaction with CO_2.

After capture from each of the three test concentrations (100%, 3.8%, 400 ppm), we rested the system in the dark for 90 min under a static N_2 headspace. As indicated also by the UV-vis absorption profile, during this time, the fluorenyl cation was gradually and completely quenched, recovering the carbinol. Thus, we considered it likely that that the captured CO_2 was fully released during the process. To confirm release, we measured the headspace CO_2 concentrations (**Figure 3e**) with a portable CO_2

meter and found a significant amount of CO_2 in the headspace, with the exact concentration depending on the dilution of the original inlet stream. In particular, we demonstrated the release 1400 ppm from the sample from direct-air capture, representing a three-fold concentration relative to the input stream. To test the cyclability of our direct capture system, we repeated the CO_2 enrichment cycle 3 times (**Figure 3f**), finding a similar effectiveness in each cycle as gauged by the amount of CO_2 outgassed in the dark.

Mechanism of CO_2 capture and release by $PB_{Me}OH$

The mechanism of hydroxide release from photoexcited **$PB_{Me}OH$** was probed by ultrafast transient absorption (TA) spectroscopy. **Figure 4a** shows the transient absorption spectrum of **$PB_{Me}OH$** after nanosecond laser excitation, using the reaction conditions of the steady-state photochemistry, namely 0.1 mM **$PB_{Me}OH$** was dissolved in 2:1 MeCN:H_2O solution. At early time delays ($\Delta t < 30$ ns), a positive TA spectrum is observed that resembles the steady-state **PB_{Me}^+** absorption spectrum shown in **Figure 3a** (trace at t = 0 min) with underlying absorption features in the 400–500 nm wavelength region. These underlying absorption features disappear at later times ($\Delta t > 300$ ns) to furnish a TA spectrum that matches the absorption spectrum of **PB_{Me}^+**. The presence of an additional species in the 400-500 nm region is supported by time-resolved decay measurements (**Figure 4a**, inset), which show that an early time species decays with a 81 ns lifetime to leave the longer-lived **PB_{Me}^+** species that persists to the maximum delay time of our detection ($\tau > 20$ ms). Normalization and subtraction of the early (9 ns) and later (90 μs) transient spectra reveals the spectrum of the early time species that is shown in **Figure 4b**.

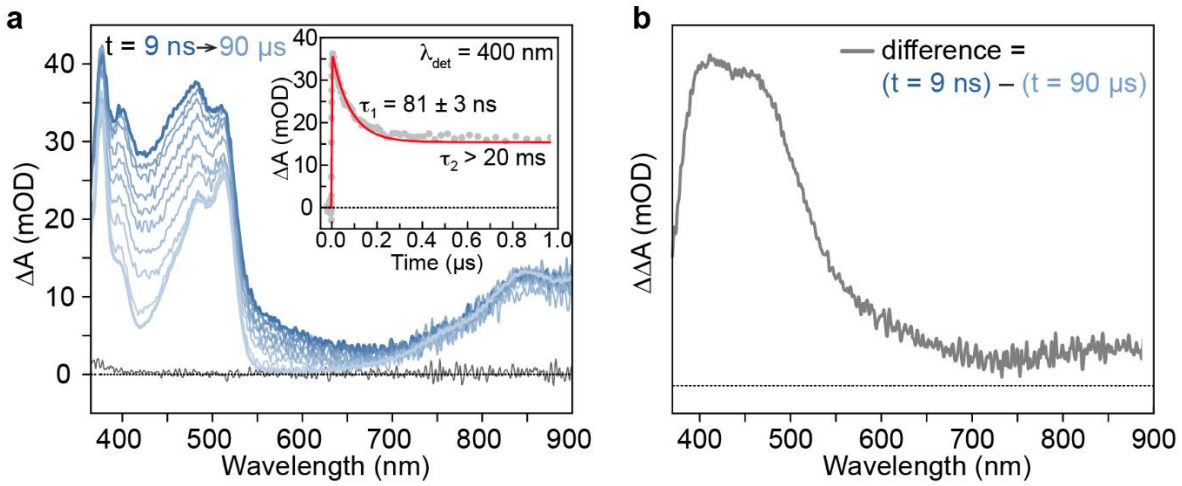

Figure 4. (a) Nanosecond TA spectra of **$PB_{Me}OH$** in 2:1 MeCN/H_2O, photoexcited at 360 nm in a 1-cm pathlength flow cuvette with a linear flow rate of 2 mL/min. Inset shows biexponential kinetics at 400 nm. (b) ΔΔA spectrum obtained by taking the difference of normalized ΔA spectra at time delays of 9 ns and 90 µs.

The identification of the early time species (**Figure 4b**) is unveiled by excited state electron transfer experiments with **$PB_{Me}Cl$**, which may be photoreduced by one electron from the excited-state of $Ru(bpy)_3^{2+}$. **Figure 5a** shows the TA spectrum resulting from the excited state quenching of $Ru(bpy)_3^{2+}$ by **$PB_{Me}Cl$**. The $Ru(bpy)_3^{2+}$ excited state (**Figure 5a**, burgundy trace) dominates the TA spectrum upon laser excitation, with a pronounced absorption and bleach with maxima of 390 and 450 nm, respectively. The TA spectrum evolves to a new species at 2.7 µs with weak absorption features centered at 425 and 550 nm, and bleach features at 450, 500 and 850 nm (**Figure 5a**, blue trace). The overall TA signal at 2.7 µs primarily comprises an absorption due to PB_{Me}• and a bleach due to the depletion of PB_{Me}^+. As shown in **Figure S15**, photoexcited $PB_{Me}Cl$ decays within 10 ps, thus only the ground state depletion of **PB_{Me}^+** contributes to the TA spectrum at 2.7 µs. **Figure 5b** shows the difference spectrum (green trace) calculated from adding the early TA feature in **Figure 4b** (reproduced as the gray trace, **Figure 5b**), the late time TA feature for **PB_{Me}^+** from **Figure 4a** (inverted as a bleaching signal as seen in **Figure 5b**, purple trace), and a small contribution of $Ru(bpy)_3^{2+}$ excited state. As shown in **Figure 5c**, the calculated difference spectrum reproduces the TA spectrum (time-averaged TA spectra from 1.2 to 1.9 µs) of $Ru(bpy)_3^{2+}$ excited state quenching by **PB_{Me}^+**, thus establishing the early time absorption spectrum in **Figure 4b** to be that of **PB_{Me}•**.

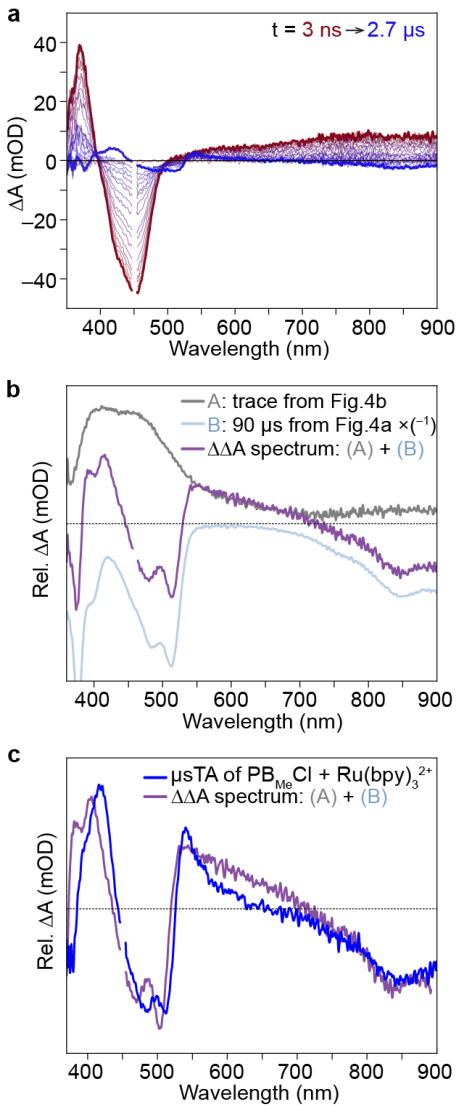

Figure 5. (a) Nanosecond TA spectra of $PB_{Me}Cl$ and $Ru(bpy)_3^{2+}$ in 2:1 MeCN/$HCl_{(aq)}$, photoexcited at 450 nm in a 1-cm pathlength cuvette. (b) Calculated spectra taken as the difference between the species from **Figure 4b** and the inversion of the 90 µs spectrum in **Figure 4a**. Not shown is a small contribution of $Ru(bpy)_3^{2+}$ excited state (burgondy spectrum from a). (c) Comparison of the royal blue spectrum from a and the calculated spectrum from b.

The presence of water is essential to furnishing long-lived $\mathbf{PB_{Me}}^+$ and $^-$OH ions, the latter of which may be captured by CO_2 to generate bicarbonate. The earliest time dynamics of $\mathbf{PB_{Me}OH}$ in neat MeCN are captured by the fsTA spectrum shown in **Figure 6a**. The absorption feature of $\mathbf{PB_{Me}}^+$ in the 600–800 nm is immediately apparent, though it is broadened when compared to the spectra in **Figure 4a**. As opposed to the extremely long ms lifetime of $\mathbf{PB_{Me}}^+$ in a MeCN/H_2O solvent mixture (**Figure 4a**, inset), the $\mathbf{PB_{Me}}^+$ transient at λ_{max} = 750 nm in neat MeCN decays by its back reaction with $^-$OH in 3.1 ns (**Figure 6b**). The later-time dynamics of $\mathbf{PB_{Me}OH}$ in neat MeCN are shown in **Figure 6c**. With the $\mathbf{PB_{Me}}^+$ species completely back-reacted with $^-$OH, a clean transient spectrum is observed for a

species that matches the ΔΔA spectrum of **PB$_{Me}$•** shown in **Figure 4b**. The **PB$_{Me}$•** radical back reacts with •OH in 35 ns (Figure 6d). The decay time constant of 3.1 ns for **PB$_{Me}^+$** in neat MeCN is consistent with observed recombination rates of solvent-caged ion pairs in polar, organic solvents,[39] thus suggesting that $^-$OH remains confined to a solvent-pair in the absence of H_2O.

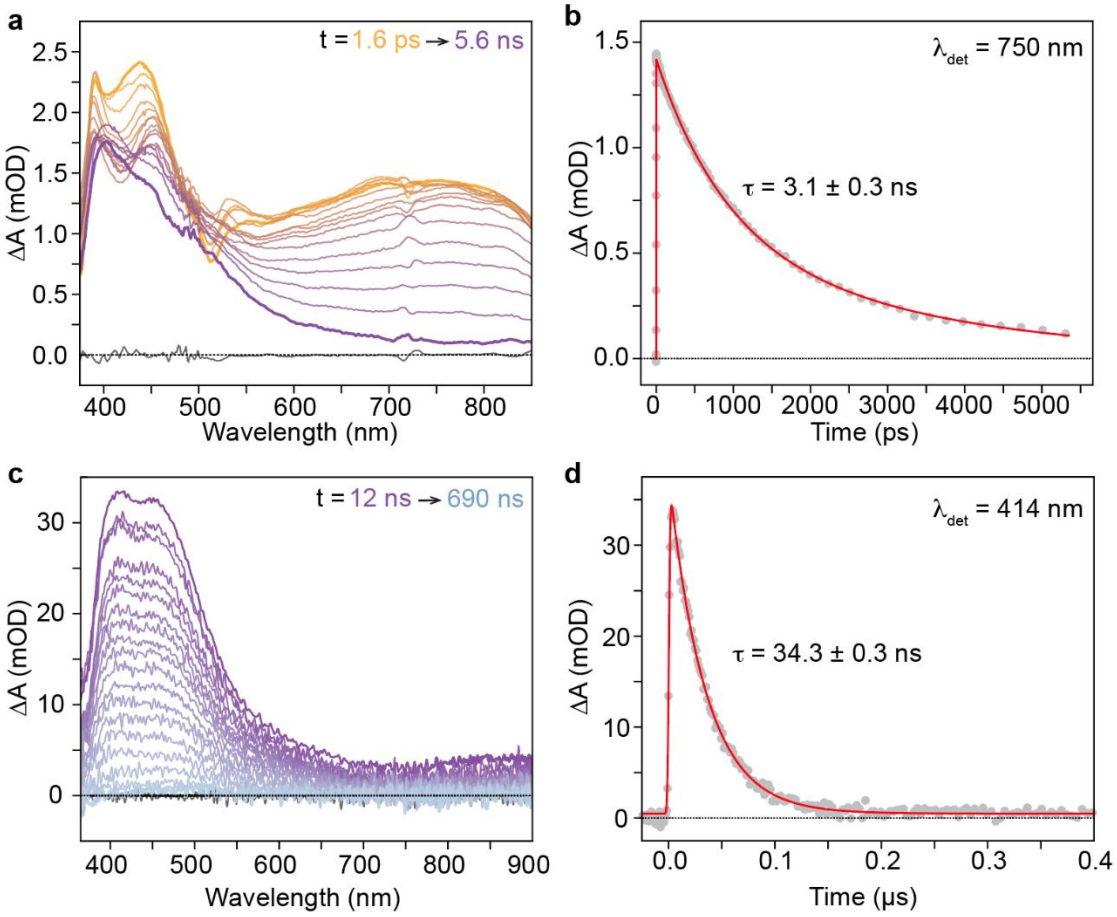

Figure 6. *Ultrafast spectroscopic characterization of **PB$_{Me}$OH** in dry MeCN.* All transient absorption (TA) presented in this figure were performed on air-equilibrated solutions of **PB$_{Me}$OH** in a 1-cm pathlength quartz cuvette with the pump laser set to 360 nm. (a) Femtosecond TA spectra of **PB$_{Me}$OH** in dry acetonitrile. (b) Kinetic traces at 750 nm (red dots) with monoexponential fits (red line). (c) Nanosecond TA spectra of **PB$_{Me}$OH** in dry acetonitrile. (d) Kinetic traces of the nsTA data at 414 nm (grey dots) with monoexponential fit (red line).

Taken together, the excited state dynamics of **PB$_{Me}$OH** are consistent with a mechanistic scheme for photochemical hydroxide release summarized in **Figure 7**. Photoexcited **PB$_{Me}$OH*** undergoes prompt bond homolysis to **PB$_{Me}$•** and •OH and bond heterolysis to **PB$_{Me}^+$** and $^-$OH within the envelope of laser excitation. The homolytic primary photoproducts recombine within 34 ns to return the system to **PB$_{Me}$OH** ground state. In the case of the primary heterolytic photoproducts, a solvent-caged [**PB$_{Me}^+$**…OH$^-$] ion pair is produced. In neat MeCN, the ion pair recombines in 3 ns. Conversely,

in the presence of H_2O, cage escape of ^{-}OH is possible. Based on the $\mathbf{PB_{Me}}^{+}$ species, persisting to $\tau >$ 20 ms, the long lifetime of the caged-escaped ^{-}OH ion enables it to be captured by CO_2 to generate the HCO_3^{-} that is observed in steady-state photolysis experiments. We note, that the cage escape yield is reflected by the production of $\mathbf{PB_{Me}}^{+}$ at long time scales (t > 1 μs), as indicated by the τ_2 kinetics decay trace shown in **Figure 4a**. Actinometric TA measurements were determined from the TA spectra at t = 2.25 μs to yield the photochemical quantum yield (QY_{PC}) of $\mathbf{PB_{Me}}^{+}$ formation (details provided in SI). We measured a QY_{PC} of 22.8 ± 0.4 %. This high quantum yield for OH^{-} photogeneration, and thus CO_2 capture, exceeds that afforded by photoacid approaches. For example, our previous investigation into merocyanine photoacids showed that productive phototriggered release of H^{+} occurred with a quantum yield of only 1.3%.

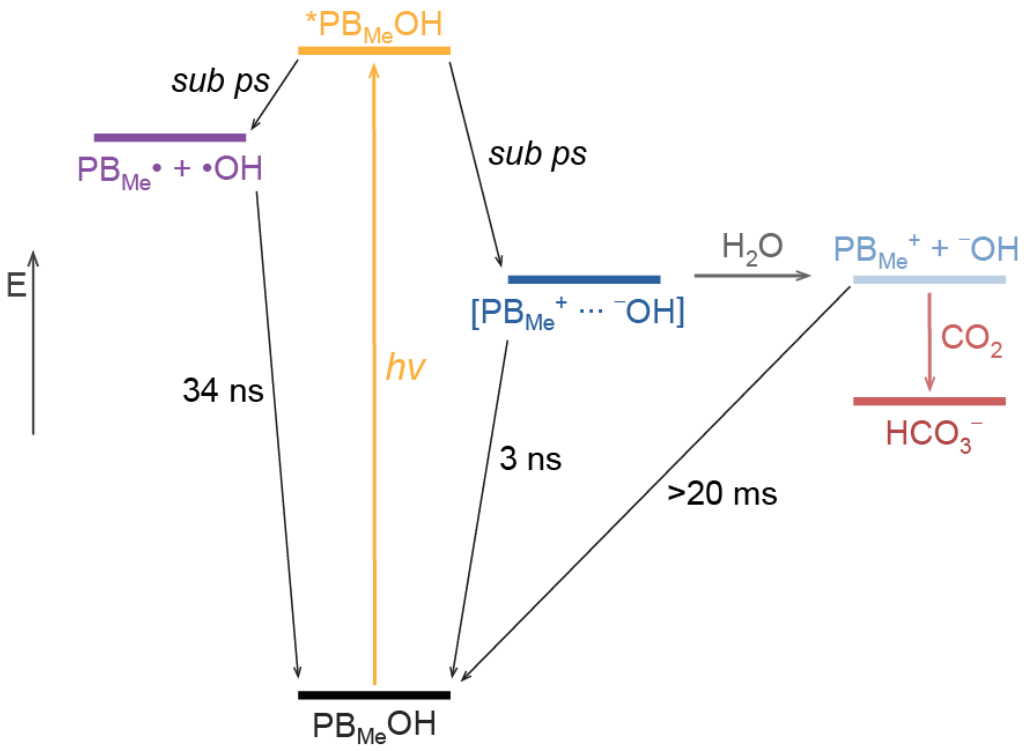

Figure 7. Homolytic (left) and heterolytic (right) bond cleavage reaction pathways from the excited state of $\mathbf{PB_{Me}OH}$. In aqueous solution, the heterolytic pathway leads to CO_2 capture when the OH^{-} cage escapes the photogenerated [$\mathbf{PB_{Me}}^{+}$…OH^{-}] ion pair.

In experiments performed under aerobic conditions, radical recombination of the homolysis products appear to outcompete degradation pathways, such as solvent reaction, as the 380–550 nm

feature returns to ground state with no other significant photoproducts observed. However, with rigorous exclusion of oxygen, nsTA experiments involving prolonged exposure to the excitation beam in 1 cm quartz cuvette produced one or more additional photoproducts (**Figure S18**). As in the photoreduction of $\mathbf{PB_{Me}Cl}$, we observe what appears to be a $\mathbf{PB_{Me}}^+$ bleach on top of another absorbing transient species. Therefore it appears that an environment free of oxygen may increase the lifetime of the $\mathbf{PB_{Me}}$• radical leading to activation of alternative photochemical pathways that compete with •OH recombination. An unusual practical consequence is that this photochemical CO_2 system not only tolerates the presence of oxygen but may require it for stability, contrasting starkly with most known electrochemical systems for which minimizing oxygen exposure is a critical consideration.

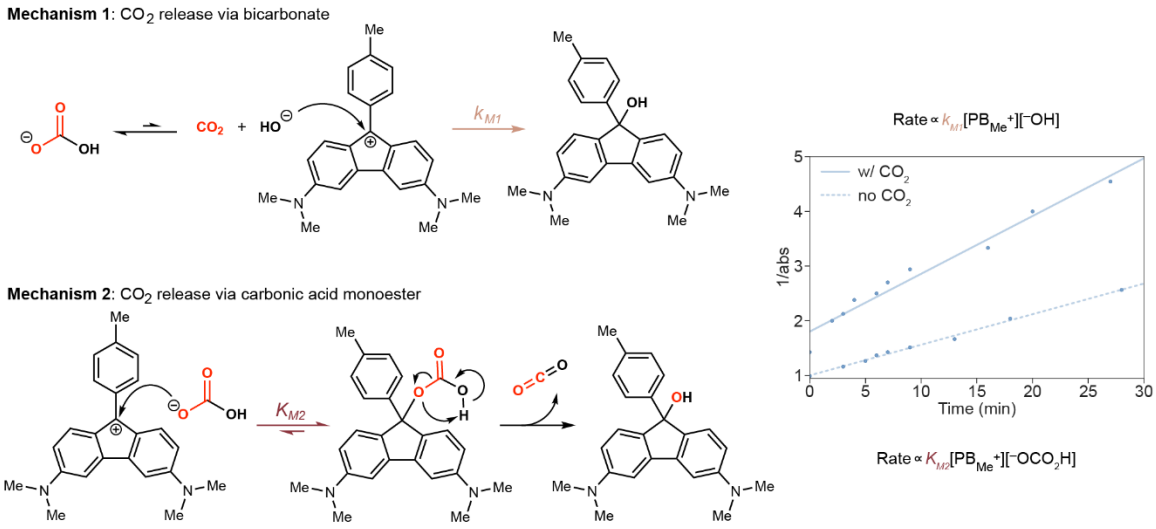

Figure 8. *Potential mechanisms of CO_2 release* Mechanism 1, CO_2 is released via carbonic acid. Mechanism 2, CO_2 is released via carbonic acid monoester. Second-order decay plot of carbocation over time with and without CO_2 10 mM MeCN-H_2O solution of $\mathbf{PB_{Me}OH}$ was stirred under 390 nm light for 5 mins. Once the light source was removed, solution aliquots were diluted to 10 μM and the UV-Vis absorption spectrum recorded to detect carbocation decay at λ ~ 950 nm over time. This was then fit to a second order rate equation and the rate constant extrapolated from the gradient of the plot shown above. This experiment was repeated but with exposure of the photobase solution to pure CO_2 under photoirradiation.

In contrast to the hydroxide release and CO_2 capture process, the CO_2 release portion of the cycle is photon-independent. Thus, its mechanistic possibilities are relatively more straightforward to analyze, and we proposed two possibilities. In mechanism 1, which is essentially the microscopic reverse of capture, the photobase is regenerated by nucleophilic attack of hydroxide, which is formed

in minor equilibrium with bicarbonate, on the carbocation. The irreversible consumption of hydroxide continuously drives bicarbonate conversion to hydroxide (and free CO_2), until all the photobase has been reconstituted and all the CO_2 released. Alternatively, in mechanism 2, the carbocation is directly attacked by its counteranion bicarbonate, producing an unstable carbonic acid monoester that rapidly dissembles by deprotonation and C–O heterolysis into photobase and free CO_2. If we assume the first step of each mechanism is involved in the rate-determining span, the predicted rate laws are, respectively:

Rate = k_{M1}[$\mathbf{PB_{Me}}^+$][$^-$OH] (mechanism 1); Rate = k_{M2}[$\mathbf{PB_{Me}}^+$][$^-$OOCOH] (mechanism 2).

A simple means to differentiate these scenarios is to compare the kinetics of release of $\mathbf{PB}^+$ $\mathbf{OH}^-$ as a reference with that of $\mathbf{PB_{Me}}^+$ $\mathbf{HCO_3}^-$. The rate of mechanism 1, linear in hydroxide concentration, should be several orders of magnitude slower with CO_2 exposure than without, as the pH of the solution decreases by several units. Using *in situ* UV-vis spectroscopy, we followed the decay of the carbocation in a *ca.* 10 mM solution of $\mathbf{PB_{Me}OH}$, prepared by photolysis, with and without pre-exposure to CO_2 (1 atm) (**Figure 8** plot). Both time courses fit well to second-order rate equations with observed rate constants of 7.01 mM^{-1} s^{-1} without CO_2 and 1.36 mM^{-1} s^{-1} after CO_2 exposure. The fact that the latter profile fits a second-order apparent rate law is evidence against mechanism 1, as the hydroxide concentration would not be directly proportional to the carbocation concentration with CO_2 present. Further, although the apparent rate is roughly 5 times lower after CO_2 exposure, we would expect a much greater decrease if the rate were directly proportional to hydroxide ion concentration. Therefore, we believe mechanism 2 is operative, and the slightly diminished rate consistent with the attenuated nucleophilicity of bicarbonate relative to hydroxide.

Thermodynamic model for photobase CO_2 capture

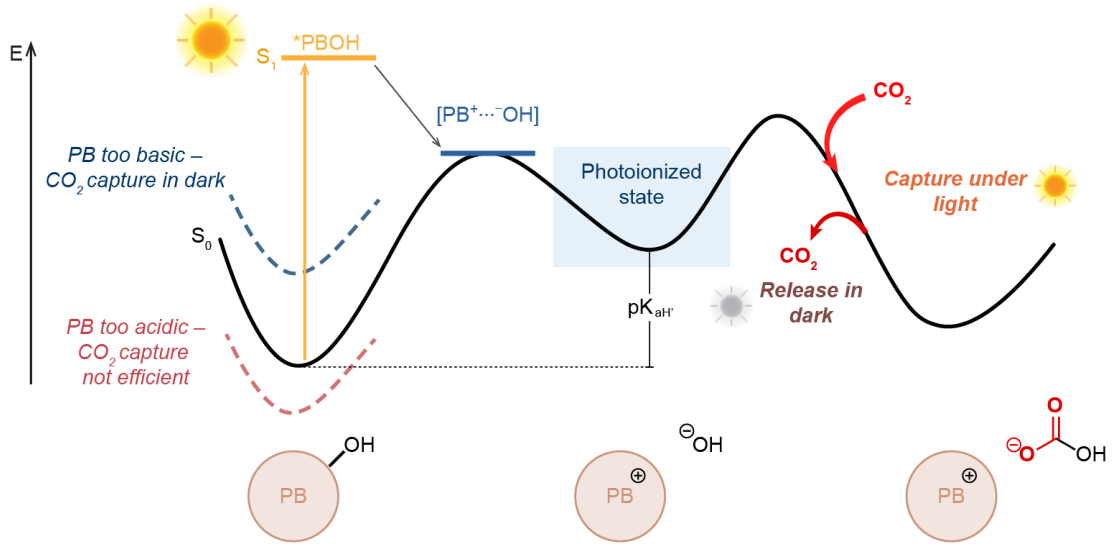

Figure 9. *Thermodynamic diagram for reversible CO_2 capture.* The photobase **$PB_{Me}OH$**, initially in the ground state, is excited (yellow arrow) to its excited state **$PB_{Me}OH$*** to produce the photoionized state according to the dynamics shown in **Figure 7**. The liberated hydroxide can capture CO_2. After the light source is removed, recombination of the ion pair back to the photobase, an energetically favourable process, drives the release of CO_2. Dashed curves highly how the ground state potential energy must be tuned to strike a thermodynamic balance for reversible CO_2 capture. If the initial photobase is too high in energy (blue), CO_2 will be captured without photoirradiation. Conversely, if the photobase is too low in energy (red), hydroxide photorelease will be less efficient, and the capacity to capture CO_2 is reduced.

Our pK_a tuning and CO_2 capture/release investigations have shown a delicate thermodynamic balance must be maintained to achieve light-driven capture and dark release (**Figure 9**). The photobase should be neutral in the dark, and hydroxide dissociation unfavourable to inhibit CO_2 capture without light. After photoexcitation the potential energy of the system is driven out-of-equilibrium resulting in favourable ionization to free hydroxide and a carbocation. The hydroxide ion can then sequester CO_2 as bicarbonate. Upon removal of the external energy stimulus, cation-hydroxide recombination is energetically favourable, and CO_2 is therefore liberated. **$PB_{Me}OH$** ($pK_{aH}' = 6.1$) was found to perform best among tested photobases, consistent with the hypothesis that the pK_{aH}' of the photobase should approximately match the pK_a of carbonic acid (6.4).

Conclusion

Our work establishes the first reversible system for CO_2 capture using Arrhenius photobases. The good performance of our new fluorenyl photobases shows that incorporation a 4π-electron ring into the carbocation can encourage excited-state hydroxide dissociation to create Baird aromaticity, yet also

favour subsequent recombination of the ground-state antiaromatic cation with hydroxide. Structure–activity relationships illustrate that the effective basicity of the photobase must be precisely tuned for efficient CO_2 separations. With the optimal system, capture was demonstrated from ambient air, followed by release into an enriched output stream. Ultrafast spectroscopic investigations show that hydroxide ion release occurs on a sub-ps timescale with high quantum efficiency. These studies suggest that photoreversible hydroxide emitters merit further investigation as tools for CO_2 capture and in other diverse applications suitably regulated by light-driven equilibria.

Acknowledgements

R.Y.L. is grateful to the Corning Fund for Faculty Development and the Salata Institute for Climate and Sustainability for partial support of this project. This work was supported by the National Science Foundation through a CAREER award to R.Y.L. (CHE-2338206), a graduate research fellowship for A.Y.W. and the Office of Naval Research (N00014-25-1-2100).

Author contributions

M.P. designed, synthesized and structurally characterized all photobases. M. P. and A.Y.W. optically characterised the photobases using UV-vis spectroscopy. M.P. performed all CO_2 experiments. A.Y.W. performed all DFT. M.C.D. designed and performed all transient absorption measurements. M.P., M.C.D., D.G.N. and R.Y.L. wrote the manuscript. All authors interpreted the results and commented on the manuscript.

Competing interests

There are no competing interests.

Additional information

Correspondence and requests for materials should be addressed to Richard Y. Liu.

Data availability

All data supporting the findings of this study are available within the article and its Supplementary Information.

References

1. Minx, J. C. *et al.* Negative emissions — Part 1 : Research landscape and synthesis. *Environ. Res. Lett.* **13**, 063001 (2018).
2. Gulev, S. K. *et al. Climate Change 2021 The Physical Science Basis Summary for Policymakers.* Ch. 1-4 (Cambridge Univ. Press, 2021).
3. Schleussner, C.-F. *et al.* Overconfidence in Climate Overshoot. *Nature* **634**, 366–373 (2024).
4. Leung, D. Y. C., Caramanna, G. & Mercedes, M. V. M. An overview of current status of carbon dioxide capture and storage technologies. *Renew. Sustain. Energy Rev.* **39**, 426–443 (2014).
5. Gibbins, J. & Chalmers, H. Carbon capture and storage. *Energy Policy* **36**, 4317–4322 (2015).
6. Hanna, R., Abdulla, A., Xu, Y. & Victor, D.G. Emergency deployment of direct air capture as a response to the climate crisis. *Nat. Commun.* **12**, 1–13 (2025).
7. Sanz-Pérez, E. S., Murdock, C. R., Didas, S. A. & Jones, C. W. Direct capture of CO_2 from ambient air. *Chem. Rev.* **116**, 11840−11876 (2016).
8. Keith, D. W., Holmes, G., St. Angelo, D. & Heidel, K. A Process for capturing CO_2 from the atmosphere. *Joule* **2**, 1573–1594 (2018).
9. Rochelle, G. T. Amine scrubbing for CO_2 capture. *Science* **325**, 1652–1654 (2011).
10. Ding, X., Chen, H., Li, J. & Zhou, T. Comparative techno-economic analysis of CO_2 capture processes using blended amines. *Carbon Capture Sci. Technol.* **9**, 100136 (2023).
11. Zito, A. M. *et al.* Electrochemical carbon dioxide capture and concentration. *Chem. Rev.* **123**, 8069−8098 (2023).
12. Wang, T., Lackner, K. S. & Wright, A. Moisture swing sorbent for carbon dioxide capture from ambient air. *Environ. Sci. Technol.* **45**, 6670–6675 (2011).
13. Lim, T. H., Foster, J. E., Ellis, B. R. & Skerlos, S. J. Microwave-based CO_2 desorption for enhanced direct air capture: experimental validation and techno-economic perspectives. *Environ. Res. Lett.* **19**, 034002 (2024).
14. Alfaraidi, A. M. *et al.* Reversible CO_2 capture and on-demand release by an acidity- matched organic photoswitch. *J. Am. Chem. Soc.* **145**, 26720−26727 (2023).
15. de Vries, A., Goloviznina, K., Reiter, M., Salanne, M. & Lukatskaya, M. R. Solvation-tuned photoacid as a stable light-driven pH switch for CO_2 capture and release. *Chem. Mater.* **36**, 1308−1317 (2024).
16. Cotton, D., Khuu, T., Takematsu, K., Delibas, B. & Dawlaty, J. M. Photoinduced carbon dioxide release via a metastable photoacid in a nonaqueous environment. *J. Phys. Chem. Lett.* **15**, 7782−7787 (2024).
17. Premadasa, U. I. *et al.* Photochemically-driven CO_2 release using a metastable-state photoacid for energy efficient direct air capture. *Angew. Chem. Int. Ed.* **62**, (2023).
18. Li, M., Irtem, E., Iglesias van Montfort, H. P., Abdinejad, M. & Burdyny, T. Energy comparison of sequential and integrated CO_2 capture and electrochemical conversion.

Nat. Commun. **13**, 1-11 (2022).

19. Sen, R. Goeppert, A., Kar S. & Prakash G. K. S. Hydroxide based integrated CO_2 capture from air and conversion to methanol *J. Am. Chem. Soc.* **142**, 4544−4549 (2020).

20. Pei, Y., Zhang, B. & Lu, Y. Next nanotechnology carbon capture and utilization via electrochemistry, what's next? *Next Nanotechnol.* **3**–**4**, 100020 (2023).

21. P Pang, S. *et al.* A phenazine-based high-capacity and high-stability electrochemical CO_2 capture cell with coupled electricity storage. *Nat. Energy*, **8**, 1126–1136 (2023).

22. Hyowon, S. & Hatton, T. A. Electrochemical direct air capture of CO_2 using neutral red as reversible redox-active material. *Nat. Commun.* **14**, 1–11 (2023).

23. Jin, S., Wu, M., Jing, Y., Gordon, R. G. & Aziz, M. J. Low energy carbon capture via electrochemically induced pH swing with electrochemical rebalancing. *Nat. Commun.* **13**, (2022).

24. Barlow, J. M. & Yang, J. W. Oxygen-stable electrochemical CO_2 capture and concentration with quinones using alcohol additives. *J. Am. Chem. Soc.* **144**, 14161−14169 (2022).

25. Wimberger, L. *et al.* Large, tunable, and reversible pH changes by merocyanine photoacids. *J. Am. Chem. Soc.* **143**, 20758−20768 (2021).

26. Wilm, L. F. B. *et al.* Photoswitchable nitrogen superbases: using light for reversible carbon dioxide capture. *Angew.Chem. Int. Ed.* **61**, (2022).

27. Sheng, W. *et al.* Proton transfer ultrafast dynamics of a " super " photobase. *Angew. Chem. Int. Ed.* **57**,14742 –14746 (2018).

28. Han, G. R. *et al.* Shedding new light on an old molecule: quinophthalone displays uncommon N-to-O excited state intramolecular proton transfer (ESIPT) between photobases. *Sci. Rep.* **7**, 1–8 (2017).

29. Yucknovsky, A. & Amdursky, N. Controlling pH-sensitive chemical reactions pathways with light - a tale of two photobases: an arrhenius and a brønsted. *Chem. Eur. J.* **30**, (2024).

30. Voegtle, M. J. & Dawlaty, J. W. Can brønsted photobases act as lewis photobases? *J. Am. Chem. Soc.* **144**, 28178−8184 (2022).

31. Gaillard, E., Fox, M. A. & Wan, P. A. kinetic study of the photosolvolysis of 9-fluorenol. *J. Am. Chem. Soc.* **111**, 2180–2186 (1989).

32. Blazek, A., Pungente, M., Krogh, E. & Wan, P. Photosolvolysis of 9-fluorenol derivatives in aqueous solution-exploratory studies of reactivity of photogenerated 9-fluorenyl cations. *J. Photochem. Photobio. A: Chem.* **64**, 315–327 (1992).

33. Chahinez, A. *et al.* A long-lived fluorenyl cation: efficiency booster for uncaging and photobase properties. *Phys. Chem. Chem. Phys.* **24**, 5294–5300 (2022).

34. Irie, M. Light-induced reversible pH change. *J. Am. Chem. Soc.* **105**, 2078–2079 (1983).

35. Uda, R. M. & Takenaka, D. Malachite green leuco derivatives as photobase generators for initiating crosslinking and polymerization. *Mater. Lett.* **303**, 130541 (2021).

36. Huajie, L. *et al.* Light-driven conformational switch of i-motif DNA. *Angew. Chem. Int. Ed.* **46**, 2515–2517 (2007).

37. Carvalho, P. C., Uzunova, D. V., Da Silva, J. P., Nau, W. M. & Pischel, U. A photoinduced pH jump applied to drug release from cucurbit[7]uril. *Chem. Commun*. **47**, 8793–8.795 (2011).

38. Hermanns, V. *et al.* Rethinking uncaging: A new antiaromatic photocage driven by a gain of

resonance energy. *Chem. Eur. J.* **27**, 14121–14127 (2021).

39. Yan, M., Lo, J. C., Edwards, J. T. & Baran, P. S. Radicals: Reactive Intermediates with Translational Potential. *J. Am. Chem. Soc.* **138**, 12692–12714 (2016).